ACS NANO

www.acsnano.org

ARTICLE

Bend-Induced Ferroelectric Domain Walls in α-In_2Se_3

Edmund Han,[⊥] Shahriar Muhammad Nahid,[⊥] Tawfiqur Rakib, Gillian Nolan, Paolo F. Ferrari, M. Abir Hossain, André Schleife, SungWoo Nam, Elif Ertekin, Arend M. van der Zande,** and Pinshane Y. Huang**

Cite This: https://doi.org/10.1021/acsnano.3c01311

ABSTRACT: The low bending stiffness of atomic membranes from van der Waals ferroelectrics such as α-In_2Se_3 allow access to a regime of strong coupling between electrical polarization and mechanical deformation at extremely high strain gradients and nanoscale curvatures. Here, we investigate the atomic structure and polarization at bends in multilayer α-In_2Se_3 at high curvatures down to 0.3 nm utilizing atomic-resolution scanning transmission electron microscopy, density functional theory, and piezoelectric force microscopy. We find that bent α-In_2Se_3 produces two classes of structures: arcs, which form at bending angles below ~33°, and kinks, which form above ~33°. While arcs preserve the original polarization of the material, kinks contain ferroelectric domain walls that reverse the out-of-plane polarization. We show that these kinks stabilize ferroelectric domains that can be extremely small, down to 2 atoms or ~4 Å wide at their narrowest point. Using DFT modeling and the theory of geometrically necessary disclinations, we derive conditions for the formation of kink-induced ferroelectric domain boundaries. Finally, we demonstrate direct control over the ferroelectric polarization using templated substrates to induce patterned micro- and nanoscale ferroelectric domains with alternating polarization. Our results describe the electromechanical coupling of α-In_2Se_3 at the highest limits of curvature and demonstrate a strategy for nanoscale ferroelectric domain patterning.

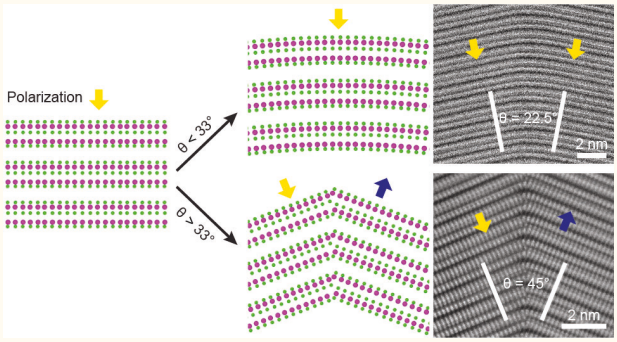

KEYWORDS: *α-In_2Se_3, van der Waals ferroelectric, ferroelectric domain wall, flexoelectricity, bending, transmission electron microscopy*

The large, switchable electric polarization of ferroelectrics makes them promising candidates for next generation technologies including energy harvesters, transducers, and memristors.[1] Flexoelectricity, defined as the coupling between strain gradients and electrical polarization, plays an important role in ferroelectrics, where it can enhance or rotate the electrical polarization and manipulate ferroelectric domain structure. For example, strain gradients from heteroepitaxy, substrate deformations, or scanned probes can be used to induce the formation of ferroelastic domain boundaries[2] and pattern ferroelectric domains.[2−9] These effects are especially significant in recently developed freestanding ferroelectrics, made by releasing epitaxially grown ferroelectric thin films like $BiFeO_3$ or by exfoliating van der Waals ferroelectrics like α-In_2Se_3. Such freestanding ferroelectrics can be bent and wrinkled into complex three-dimensional shapes. Understanding the interaction between mechanical deformation and ferroelectric polarization in this regime of highly deformed structures is important to emerging applications like nanoscale transducers or sensors, microrobotics, and wearable electronics.

In particular, flexoelectricity has emerged as an active area of research in 2D van der Waals materials,[10−14] because their high fracture stress[15,16] and low bending moduli[17−20] make it possible to sustain extremely large strains and strain gradients. van der Waals materials can achieve bending radii as low as 1 nm,[19,20] more than 30-fold higher curvatures than those achieved so far in freestanding ferroelectric oxides, corresponding to strain gradients 2 orders of magnitude higher than those achieved via heteroepitaxy in conventional thin film oxides. While flexoelectric effects should be strongest in strongly polar

Received: February 10, 2023
Accepted: April 10, 2023

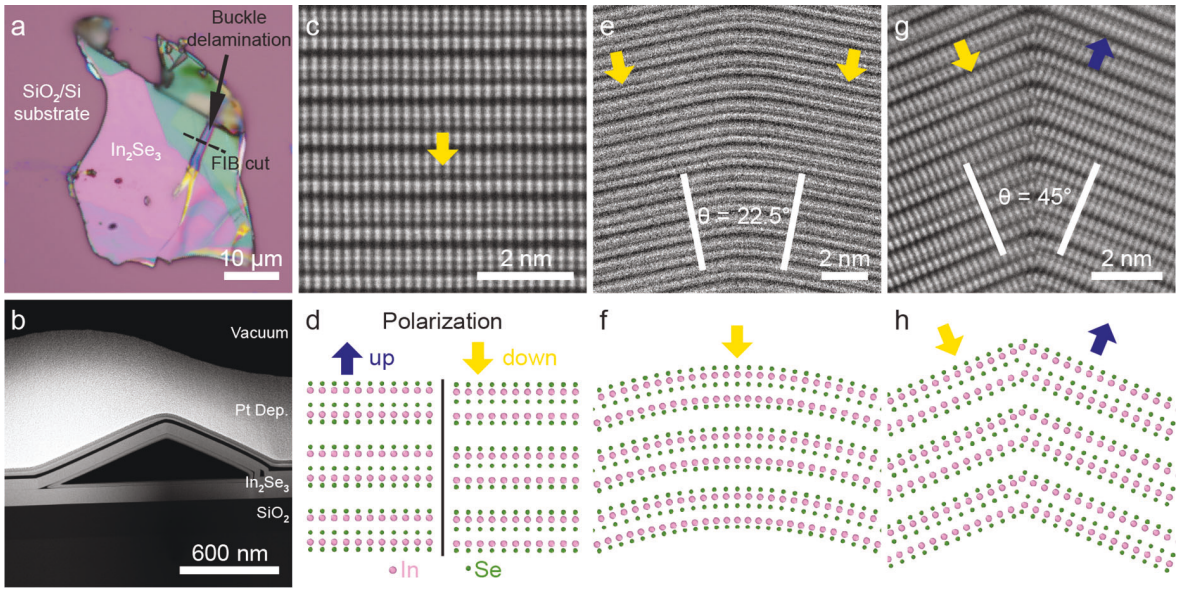

Figure 1. Bend-induced domain wall formation in α-In_2Se_3. (a) Optical image of α-In_2Se_3 flake mechanically exfoliated onto a SiO_2/Si substrate. (b) Cross-sectional ADF-STEM image of the α-In_2Se_3 buckle, from the region indicated by the dotted line in (a). (c) ADF-STEM image and (d) cartoon of flat multilayer α-In_2Se_3, viewed along the $\langle\bar{1}100\rangle$ zone axis. The out-of-plane polarization is visible as a shift in the center Se layer in each quintuple layer of α-In_2Se_3 and is directly determined from atomic-resolution imaging. (e) ADF-STEM image and (f) cartoon of an arc in multilayer α-In_2Se_3, with a bending angle of 22.5°. The polarization varies smoothly with the curve and points downward, perpendicular to the basal plane on both sides of the arc. (g) ADF-STEM image and (h) cartoon of a kink with a bending angle of 45°. The polarization changes from *down* to *up* across the kink from left to right.

materials such as ferroelectrics, the vast majority of studies in 2D systems have focused on materials that are centrosymmetric or weakly polar. The interplay between high strain gradients and ferroelectricity remains largely unexplored.

Here, we investigate the impact of nanoscale bending in α-In_2Se_3, a room-temperature van der Waals ferroelectric with a thickness-dependent Curie temperature of 533−700 K.[21−23] α-In_2Se_3 has been used in field-effect transistors, memristors, neural computing, and nonvolatile memories.[24] Moreover, α-In_2Se_3 exhibits rich electromechanical behavior, such as strain-induced phase changes[25] and flexoelectric effects.[10] We utilize bending in α-In_2Se_3 to probe electromechanical coupling in a previously unstudied limit: in a strongly polarized, ferroelectric material under extreme bending down to a 0.3 nm radius of curvature, where electromechanical coupling should be the strongest. By combining atomic-resolution scanning transmission electron microscopy (STEM) with density functional theory (DFT) and piezoelectric force microscopy (PFM), our work provides an atomic-scale understanding of bending in 2D ferroelectrics and illustrates a mechanism by which bending leads to the formation of ferroelectric domain boundaries in 2D systems.

RESULTS AND DISCUSSION

Figure 1 demonstrates the impact of bending and the formation of bend-induced domain walls in multilayer α-In_2Se_3. Figure 1a shows an optical image of a typical sample containing a bend. To induce bends, we mechanically exfoliate α-In_2Se_3 onto a SiO_2/Si substrate (see Section 1.1 in the Supporting Information). Many of the flakes naturally contain buckle delaminations, which form due to stresses induced during exfoliation, as has been observed in other van der Waals materials.[26−29] Then, we prepare cross-sections of the buckle using focused ion beam (FIB) milling and image the samples using aberration-corrected annular dark-field STEM (ADF-STEM). We use ADF-STEM to image the microscale morphology of the buckle, characterize the nanoscale curvature of an individual bend, and probe the atomic-scale structure within each layer in order to determine the local polarization of the ferroelectric. Figure 1b is a micron-scale STEM image showing each buckle contains several nanoscale bends. Figure 1c shows the local atomic structure within the ferroelectric at a flat region near the buckle. As shown in Figure 1d, the crystal structure of α-In_2Se_3 possesses a net out-of-plane electric dipole moment. This polarization can be seen as a shift of the center Se sublayer along the *c*-axis within each quintuple layer[21,22,30] and imaged via cross-sectional atomic-resolution STEM (Figure 1c). We further confirm the polarization direction with PFM (Figure S1). While some groups have also reported an in-plane polarization component,[31,32] α-In_2Se_3 exhibits 3-fold rotational crystal symmetry (Figure S2), which should produce zero net in-plane polarization in the absence of in-plane strain.[33]

As shown in Figure 1e−h, we observe two classes of bends—arcs and kinks. These structures are distinguished by their bending radii: while kinks are atomically sharp, we observe arcs with internal bending radii of 5−150 nm. At the bends, we sometimes observe buckle delamination, where layers of α-In_2Se_3 separate (Figure 1b), but we do not observe the formation of cracks within a layer at any of the arcs or kinks. Figure 1 panels e and f show the ADF-STEM image and cartoon structure of an arc with a bending angle of 22.5°. While atomic columns are not visible in Figure 1e because the bending direction does not lie along a major zone axis, the polarization direction is still visible by examining the shifts of the center Se plane in each α-In_2Se_3 layer. The polarization direction rotates smoothly with the curve, pointing toward the substrate (*down*) across the entire arc and remaining

https://doi.org/10.1021/acsnano.3c01311
ACS Nano XXXX, XXX, XXX−XXX

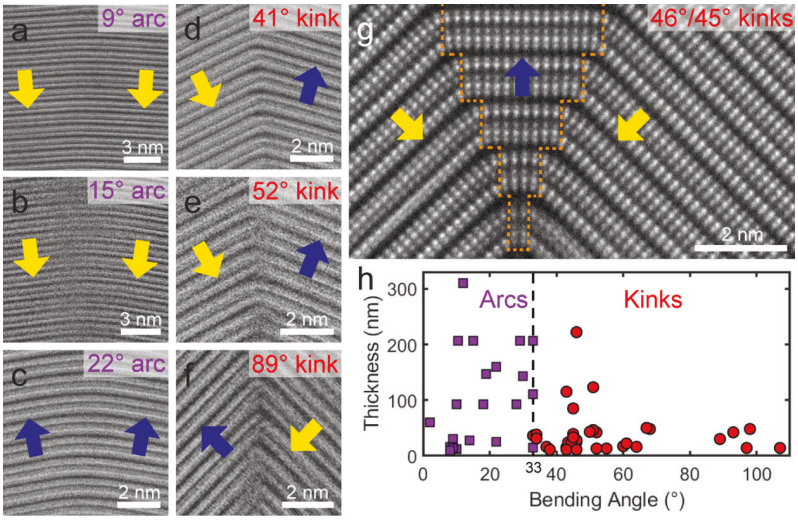

Figure 2. Angle-dependent kink and domain wall formation. (a–f) ADF-STEM images of six different bends in multilayer α-In_2Se_3. Smooth arcs (purple) contain no domain walls, whereas sharp kinks (red) exhibit domain walls. (g) ADF-STEM image of two kinks in series, resulting in a wedge-shaped domain polarized *up* between two domains polarized *down*. At the tip of the wedge, the domain width within a layer drops to only two atoms wide. (h) Plot of multilayer thickness versus bending angle for arcs (purple squares) and kinks (red circles), extracted from 55 different bends. For samples where a portion of the material delaminates to form a bend; the thicknesses are reported for the delaminated layers. Arcs occur for bends below 33°, while kinks form above 33°.

perpendicular to the basal plane. Figure 1 panels g and h show an ADF-STEM image and cartoon structure of a kink with a bending angle of 45°. The kink forms an atomically sharp domain wall. Across the kink, the polarization changes from pointing roughly *down* toward the substrate to *up* away from the substrate, while remaining perpendicular to the basal plane on either side.

In Figure 2, we systematically investigate the role of bending angle on the sample morphology. Figure 2 panels a–f show STEM images from six bends with bending angles from 9° to 89°. Generally, smaller bending angles (ex: 9°, 15°, and 22° bends shown in Figure 2a–c) produce smooth arcs, while larger bending angles (ex: 41°, 52°, and 89° bends shown in Figure 2d–f) produce kinks. Moreover, we do not observe any strain away from the kink. In addition, arcs do not contain any defects, such as dislocations or disclinations, and they do not appear to alter the polarization direction of the material: for example, the bends in Figure 2a–c can appear in both *down* (Figure 2a,b) and *up* (Figure 2c) domains. These structures achieve extremely high strain gradients. For example, the strain gradient in the arcs, calculated as the reciprocal of the radius of curvature, ranges between 7×10^6 and 2×10^8 m^{-1}, 2 orders of magnitude higher than in heteroepitaxial growth[2] and 12 to 400 times higher than in atomic force microscopy (AFM) tip-induced mechanical writing.[34−36]

Notably, we also find that kinks in mechanically deformed α-In_2Se_3 can produce extremely small ferroelectric domains. The STEM image in Figure 2g shows two kinks in close proximity, resulting in a wedge-shaped *up* domain in between two domains polarized *down*. At the tip of the wedge, the domain is only two atoms (approximately 4 Å) wide. To our knowledge, this is the smallest dimension ever reported for a ferroelectric domain, 75 times smaller than the domains obtained from an AFM probe-induced strain gradient.[6]

Figure 2h plots the thickness of the α-In_2Se_3 versus bending angle for arcs (purple squares) and kinks (red circles) in 55 bends measured across 9 different samples. Two trends are visible in these data: first, lower bending angles <33° produce smooth arcs, while higher bending angles >33°, lead to sharp kinks. This behavior is thickness-independent and consistent across the 55 bends measured. Second, kinks produce an atomically sharp domain wall, while arcs do not.

These observations are strikingly different from the flexoelectric effects previously observed in 2D materials, where the polarization is directly correlated with the sign of the local curvature. For example, periodic ferroelectric striped domains form in rippled $CuInP_2S_6$, where the polarization points radially outward with respect to each curve.[4] Bend-induced flexoelectricity has also been observed in nonferroelectric 2D materials such as graphene, MoS_2, and other 2D transition metal dichalcogenides.[11−14] In contrast, our images show that arcs of α-In_2Se_3 maintain their original polarization direction with respect to the *c*-axis, with no measurable shifts in the center Se sublayer, regardless of whether the polarization points radially inward or outward. Rather than direct flexoelectricity in smooth arcs, kink formation is the primary mechanism for bend-induced ferroelectric domain wall formation in α-In_2Se_3.

Figure 3 identifies the energetic and geometric origins of kink formation. Figure 3a shows the relaxed structures of a monolayer α-In_2Se_3 arc and kink obtained from DFT. In these simulations, we vary the bending angle by changing the compression of the supercell. Next, using methods we have developed to study bending in van der Waals multilayers and heterostructures,[19,20] we measure the bending energy, defined as the difference in ground state energies between bent and flat structures of equal length. To match experiment, we initialize the kinks with a domain wall and arcs without a domain wall (Figure S3 and Section 1.2 in the Supporting Information). We also simulate kinks without domain walls but find that such structures are energetically unfavorable (Section 1.3 in the Supporting Information). We calculate the bending stiffness of monolayer α-In_2Se_3 to be 9.9 ± 0.2 eV (Section 1.4 in the Supporting Information), on the same order of the bending stiffnesses of monolayer transition metal dichalcogenides.[17,20,37,38]

https://doi.org/10.1021/acsnano.3c01311
ACS Nano XXXX, XXX, XXX−XXX

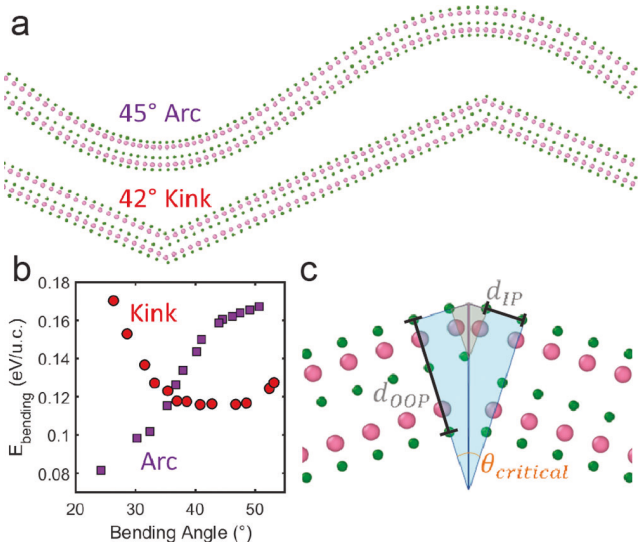

Figure 3. Calculated structure and energetics for arc and kink formation in α-In_2Se_3. (a) Simulated relaxed structures of monolayer arc and kinks obtained from DFT simulations at 45° and 42° bending angles, respectively, with bending axes parallel to the $\langle\bar{1}100\rangle$ direction. (b) Plot of DFT-calculated bending energy versus bending angle for arcs (purple) and kinks (red) in α-In_2Se_3. At bending angles above approximately 36°, kinks are more energetically stable than arcs. (c) Wedge disclination illustration in the kink. The geometric relationship requires a bending angle of 34° to satisfy the formation of one disclination per layer.

Figure 3b plots the bending energy for arcs and kinks as a function of bending angle from DFT. Here, we focus on bending angles near 33° to understand the origin of the observed transition from arcs to kinks. For arcs, the bending energy increases with angle, as expected from continuum mechanics.[39,40] In contrast, the bending energy of kinks exhibits a minimum between 35° and 45° (details in Figure S4 and Section 1.5 of the Supporting Information). Importantly, Figure 3b shows that the bending energies of arcs and kinks cross at a bending angle of approximately 36°, making arcs energetically favorable below this angle and kinks favorable above it. These results are in excellent agreement with the experimental data in Figure 2.

The origin of this critical bending angle can be understood using the theory of geometrically necessary disclinations.[41] The diagram in Figure 3c relates the bending angle required to form one disclination per layer in a kink to the lattice parameters of α-In_2Se_3. This diagram indicates an "ideal" bending angle to form a kink from a disclination with minimal lattice strain: $\theta_{critical} = 2\cdot \arctan\left(\frac{d_{IP}}{d_{OOP}}\right)$, where d_{IP} = 2.08 Å is the in-plane spacing between projected atomic columns, and d_{OOP} = 6.70 Å is the distance between the top and bottom Se planes, acquired from DFT simulations. This equation yields an equilibrium kink angle of 34° for a crystal bent parallel to the $\langle\bar{1}100\rangle$ direction. While the geometric condition for disclination formation should depend on the crystallographic direction of the bend, our calculations yield a similar critical angle for bending along the $\langle\bar{2}100\rangle$ zone axis (Figure S5). Here, these angles represent the bending angles for which kink formation energy should be the lowest, and they are in good agreement with our DFT results. Interestingly, the formation of domain walls via disclination kinks creates a purely geometric condition for the bend-induced domain walls in α-In_2Se_3, a phenomenon that has not been previously observed in other ferroelectrics.

Next, we show how 3D buckled structures generate micron-scale polarization domains. Figure 4 shows corresponding low-magnification ADF-STEM, AFM topography, and PFM images of an α-In_2Se_3 buckle formed via mechanical exfoliation (see Methods for PFM imaging details). The buckle structure is complex, containing multiple arcs and kinks (Figure 4a). Because each kink produces a domain wall, buckles that contain an odd number of kinks in series have opposite polarization on either side. In Figure 4a, three kinks are visible (black solid lines) in the layers near the top of the sample.

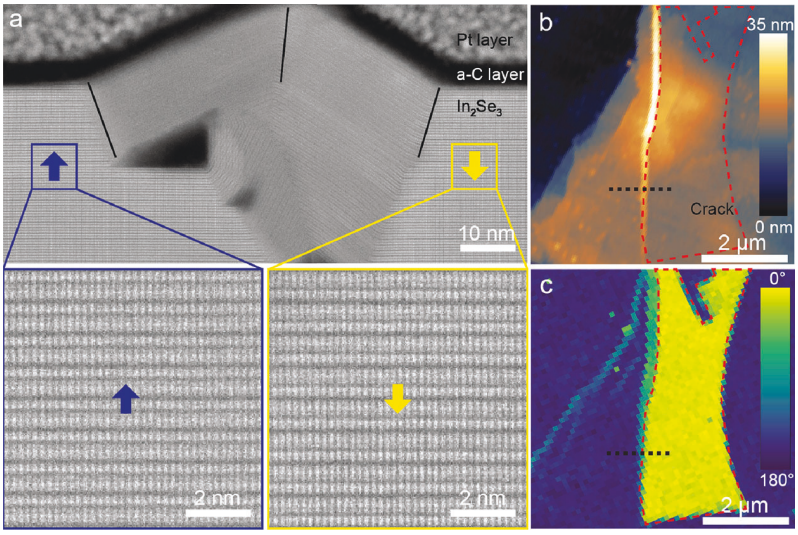

Figure 4. Domain evolution at buckles in α-In_2Se_3. (a) Cross-sectional ADF-STEM image of a complex α-In_2Se_3 buckle. Layers undergo three kinks in series as marked by the solid black lines, producing opposite polarizations to the left and right of the buckle. (b) AFM height image and (c) normal PFM phase image of the same α-In_2Se_3 flake shown in (a). The bright gold vertical line in (b) is the buckle in the flake. As shown in (c), the majority of the flake has an upward polarization (blue), except to the right of the buckle, where there is a ~2 μm wide downward-polarized ferroelectric domain (yellow). The boundary of the new domain is marked by the red dashed line.

https://doi.org/10.1021/acsnano.3c01311
ACS Nano XXXX, XXX, XXX−XXX

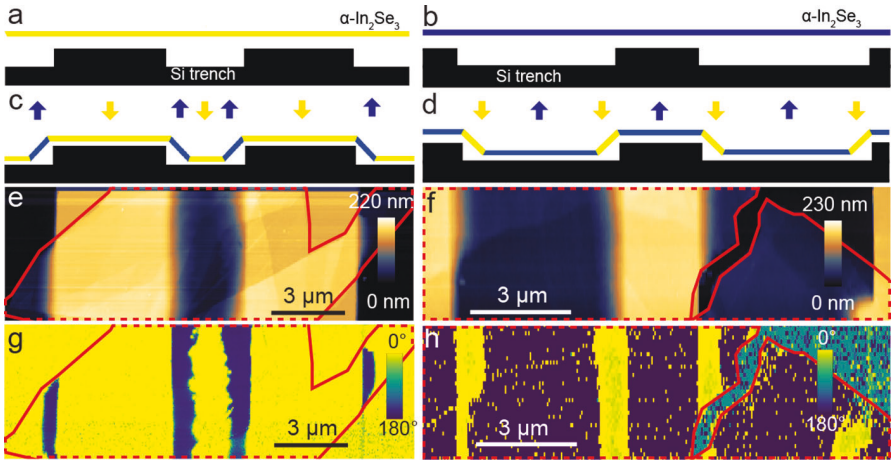

Figure 5. Controlled domain wall formation in α-In_2Se_3 using patterned substrates. (a–d) Schematics of the experiment before (a,b) and after (c,d) transfer. (e,f) AFM height profile of Sample 1 and Sample 2 transferred on the trenches and (g,h) corresponding PFM phase images, with the edges of the flakes marked in red. Sample 1 in (e) has an initial polarization *down*, while Sample 2 in (f) has an initial polarization *up*. After transfer, flat regions maintain the original polarization direction, while suspended α-In_2Se_3 at the trench edges exhibit reversed polarization.

Comparing the AFM and PFM images (Figure 4b,c), we see that, while the majority of the flake has an upward (blue) polarization, a new domain (yellow) starts at the buckle and propagates around 2 μm to the right, until it terminates at a crack in the material (Figure S6 shows STEM images of the crack). We observe this domain creation and termination in several samples; in each, the newly generated domain propagates freely through the material until it is arrested by a defect such as an edge, crack, or another kink. These data suggest that kinks may be used to controllably fabricate ferroelectric domains.

Figure 5 demonstrates the controlled creation of ferroelectric domains in α-In_2Se_3 using templated substrates. Templated substrates have been utilized to apply patterned strains and strain gradients in order to explore physics such as strain engineering of Raman modes,[42] exciton trapping,[43] and inducing of superlattice quantum states.[44] We use electron beam lithography to fabricate an array of trenches 2–5 μm wide and 150 nm deep in a Si substrate and then transfer 12–40 nm α-In_2Se_3 flakes on top (see Methods). The trenches serve as a template on which the α-In_2Se_3 partially conforms to the surface. Using our previous studies of 2D materials laminated on steps,[19,20] we estimate the thickness-dependent bending stiffness of α-In_2Se_3 and design the height of the trenches to promote the formation of kinks in thin samples (Section 1.7 in the Supporting Information and Figure S9). Before transfer, the α-In_2Se_3 flakes have uniform polarization *down* (Figure 5a) or *up* (Figure 5b). AFM topography images (Figure 5e,f) and corresponding PFM phase images (Figure 5g,h) are shown for two representative samples (see Figure S7 for optical microscope images of the samples and Figure S8 for an additional sample). Sample 1 (Figure 5e,g) is 25 nm thick, while Sample 2 (Figure 5f,h) is 20 nm thick. After transfer, each flake forms two domain wall kinks near the edges of each trench: one at the top and one at the bottom of each trench. The PFM data (Figure 5 g,h) show that flat regions of the sample maintain the original polarization direction of the flake, while suspended regions at the edge of the trenches have reversed polarization. Discussed in the Supporting Information Section 1.6, we estimate that the primary contribution to the PFM signal on the suspended regions is the piezoelectric expansion of the film, with smaller contributions rising from the electrostatic and flexoelectric deflection. We also observe that the domain wall at the top of the step is straight, whereas the domain wall at the bottom of the step is jagged (Figure 5g,h and Figure S8). The roughness of the domain wall at the bottom of the trench likely results from heterogeneities in the local strain within the α-In_2Se_3 flake after transfer, which produces variations in the position of the contact between the material and the substrate and thus the location of the kink and domain wall. Together, Figure 5 demonstrates that the bend-induced polarization reversal can be directly induced and patterned using templated substrates. Modifying the size and aspect ratio of the templated surface should allow patterning of domains with different shape, size and symmetry. Coupled with our observations in Figure 2g, the minimum size of patterned ferroelectric domains in α-In_2Se_3 may be as low as 4 Å, nearly 2 orders of magnitude smaller than the domain size obtained from utilizing an AFM probe-induced strain gradient.[6]

CONCLUSION

These results demonstrate a mechanism in α-In_2Se_3, where bending to high angles produces kinks and corresponding ferroelectric domain walls. We experimentally observe a critical bending angle for kink formation, which we corroborate using DFT calculations and the theory of geometrically necessary disclinations. We also show that new ferroelectric domains are nucleated from these kinks and propagate over the micron scale. Finally, we demonstrate that we can pattern micron-scale ferroelectric domains by transferring multilayer α-In_2Se_3 to templated substrates. This study provides a fundamental understanding of bend-induced atomic-to-micron-scale structural modulation that produces electrical polarization domain boundaries in van der Waals ferroelectrics. These findings establish opportunities for electrical polarization manipulation and domain wall engineering in deformable nanoelectronics.

METHODS

TEM Sample Preparation. We thermally evaporate a protective layer of amorphous carbon that is 5–30 nm thick on top of α-In_2Se_3. Then, we fabricate cross-sectional STEM samples using standard FIB

https://doi.org/10.1021/acsnano.3c01311
ACS Nano XXXX, XXX, XXX–XXX

lift-out procedures in a Thermo Fisher Scientific Helios 600i DualBeam FIB-SEM and Scios 2 DualBeam FIB-SEM. A cryo-can is used during thinning to minimize redeposition.

Aberration-Corrected STEM Imaging. The cross-sectional samples are imaged in a Thermo Fisher Scientific Themis Z aberration-corrected STEM. The STEM is operated at 300 kV at a convergence angle of 25.2 mrad.

DFT Simulations. We use DFT to simulate bending in monolayer α-In_2Se_3 using VASP[45] with projector augmented wave pseudopotentials.[46] The in-plane lattice constant of the In_2Se_3 unit cell is 4.1 Å and its thickness is 6.7 Å. We choose a rectangular supercell of monolayer In_2Se_3 that contains 400 atoms. To bend the monolayer α-In_2Se_3, we deform the material through geometric perturbation in the out-of-plane z-direction. We also reduce the size of the simulation cell along the x-direction so that the total length of the deformed α-In_2Se_3 remains the same as its flat configuration. The y-direction remains unchanged and parallel to the xz-plane. The dimension of the system size of the simulation is 166.47 Å × 7.21 Å × 58 Å. We incorporate a vacuum of 58 Å to avoid interaction between the adjacent periodic image of α-In_2Se_3 along the z-direction. To generate the bend structures, we have followed the methodology from our previous papers.[19,20]

The Brillouin zone is integrated using the Monkhorst−Pack method[47] and the k-space is sampled using a 1 × 4 × 1 mesh. The energy cutoff for the DFT simulations is 400 eV for the plane wave basis and 10^{-4} eV for the total energy convergence. Geometric relaxations are performed to obtain the ground state configuration for each α-In_2Se_3 supercell. We allow the relaxation until forces on each atom are below 0.03 eV/Å. We calculate the bending energy of bent α-In_2Se_3 by subtracting the total energy of the unstrained and flat configuration from the total energy of bent configuration. From the bending energy, we also calculate the bending stiffness of monolayer α-In_2Se_3 which is 9.9 ± 0.2 eV (see Section 1.4 in the Supporting Information), consistent with the bending stiffnesses of monolayer transition metal dichalcogenides.[17,20,37,38]

PFM Imaging. We perform AFM and PFM imaging with an AIST-NT SmartSPM instrument. During the measurement, we apply an AC bias to the platinum coated probe (ElectriTap190-G, Budget Sensor) at the contact resonance frequency. We measure in PFM-Top Mode where the probe is in contact with the sample during the measurement but lifted in between two scanning points to minimize probe wear and parasitic signals. For each scanning point, the piezoelectric flake oscillates in response to the oscillating electric field generated by the applied AC bias on the probe. The cantiliever deflects in response to the oscillation. which is captured by a lock-in amplifier. The phase and amplitude of the deflection along with the topography is obtained by PFM. The phase image shows the orientation of the dipole moments of the sample.

Fabrication of Patterned Trenches. To fabricate the array of trenches, 400 nm of ZEP is spin-coated on Si substrate. Then the design of the trenches (length 50 μm and width 2 μm with 5 μm separation for sample 1; length 50 μm and width 5 μm with 2 μm separation for sample 2 and length 50 μm and width 5 μm with 1 μm separation for sample 3) is patterned by electron beam lithography. Then the ZEP is developed and the Si substrate is etched to create 150 nm deep trenches by CHF_3 etchant. The remaining ZEP is removed by PG remover and the substrate is subsequently sonicated and cleaned by Piranha solution to remove any possible polymer residue. **Caution**: Piranha solution is aggressive and explosive. Never mix Piranha waste with solvents. Check the safety precautions before using it.

Transfer of α-In_2Se_3. First, the α-In_2Se_3 flakes are exfoliated on SiO_2 substrate. Then, a 6% (w/w) poly(bisphenol A carbonate) (PC) in chloroform is spin-coated on the substrate. The PC film, along with the α-In_2Se_3, is subsequently delaminated and put on a polydemethylsiloxane (PDMS) stamp. Finally, the PC film along with the α-In_2Se_3 flake is transferred onto the trenches and the temperature is increased to 200°. The PC melts and is removed by putting the whole system in an overnight chloroform bath.

ASSOCIATED CONTENT

Data Availability Statement

The data of this study may be accessed in the Illinois Data Bank repository, https://doi.org/10.13012/B2IDB-1187822_V1.

Supporting Information

The Supporting Information is available free of charge at https://pubs.acs.org/doi/10.1021/acsnano.3c01311.

Information on (1) mechanical exfoliation and characterization of α-In_2Se_3, (2) geometry of arcs and kinks in DFT, (3) additional discussion of polarization switch due to kink, (4) calculation of bending stiffness of α-In_2Se_3, (5) explanation of the variation of bending energy with bending angle, (6) origin of PFM contrast of α-In_2Se_3 on Si trenches, (7) designing the height of trenches; Figures S1−S9 showing PFM images, cartoon structure showing zero net in-plane polarization, atomic representation of the structures used for DFT, DFT simulations of curvature along the arc and kink, STEM image of a kink bent along the <$\bar{2}$210> zone axis, STEM images showing the termination of new domain, optical microscope images of samples 1 and 2, controlled polarization switching in sample 3, model estimating the step height of the trench from bending geometry (PDF)

AUTHOR INFORMATION

Corresponding Authors

Arend M. van der Zande − *Department of Mechanical Science and Engineering and Materials Research Laboratory, University of Illinois Urbana−Champaign, Urbana, Illinois 61801, United States;* orcid.org/0000-0001-5104-9646; Email: arendv@illinois.edu

Pinshane Y. Huang − *Department of Materials Science and Engineering, University of Illinois Urbana−Champaign, Urbana, Illinois 61801, United States; Materials Research Laboratory, University of Illinois Urbana−Champaign, Urbana, Illinois 61801, United States;* orcid.org/0000-0002-1095-1833; Email: pyhuang@illinois.edu

Authors

Edmund Han − *Department of Materials Science and Engineering, University of Illinois Urbana−Champaign, Urbana, Illinois 61801, United States;* orcid.org/0000-0002-1910-9052

Shahriar Muhammad Nahid − *Department of Mechanical Science and Engineering, University of Illinois Urbana−Champaign, Urbana, Illinois 61801, United States;* orcid.org/0000-0002-0049-6152

Tawfiqur Rakib − *Department of Mechanical Science and Engineering, University of Illinois Urbana−Champaign, Urbana, Illinois 61801, United States;* orcid.org/0000-0001-6903-6667

Gillian Nolan − *Department of Materials Science and Engineering, University of Illinois Urbana−Champaign, Urbana, Illinois 61801, United States;* orcid.org/0000-0003-2356-9075

Paolo F. Ferrari − *Department of Mechanical Science and Engineering, University of Illinois Urbana−Champaign, Urbana, Illinois 61801, United States*

M. Abir Hossain − *Department of Mechanical Science and Engineering, University of Illinois Urbana−Champaign,*

https://doi.org/10.1021/acsnano.3c01311
ACS Nano XXXX, XXX, XXX−XXX

Urbana, Illinois 61801, United States; orcid.org/0000-0003-1606-5960

André Schleife − *Department of Materials Science and Engineering, University of Illinois Urbana−Champaign, Urbana, Illinois 61801, United States;* orcid.org/0000-0003-0496-8214

SungWoo Nam − *Department of Mechanical and Aerospace Engineering, University of California, Irvine, Irvine, California 92697, United States; Department of Materials Science and Engineering, University of California, Irvine, Irvine, California 92697, United States;* orcid.org/0000-0002-9719-7203

Elif Ertekin − *Department of Mechanical Science and Engineering and Materials Research Laboratory, University of Illinois Urbana−Champaign, Urbana, Illinois 61801, United States;* orcid.org/0000-0002-7816-1803

Complete contact information is available at: https://pubs.acs.org/10.1021/acsnano.3c01311

Author Contributions

[⊥]E.H. and S.M.N. contributed equally to this work

Author Contributions

Under P.Y.H.'s supervision, E.H. and G.N. performed TEM sample preparation and STEM imaging and analysis. Under P.Y.H.'s, A.M.v.d.Z.'s, and E.E.'s supervision, E.H., S.M.N., and T.R. developed mechanics modeling and analysis. Under E.E.'s supervision, T.R. performed DFT calculations. Under A.M.v.d.Z's and S.W.N.'s supervision, S.M.N. performed AFM and PFM measurements. Under P.Y.H.'s, A.M.v.d.Z.'s, and A.S.'s supervision, E.H., S.M.N., G.N., P.F.F., and M.A.H. performed sample preparation of buckled structures. All authors read and contributed to the manuscript.

Notes

The authors declare no competing financial interest.

ACKNOWLEDGMENTS

This work was primarily supported by NSF-MRSEC under Award Number DMR-1720633. This work was also supported by the Air Force Office of Scientific Research under grant No. FA9550-20-1-0302 and the Office of Naval Research under grant No. N00014-18-1-2605. This work was carried out in part in the Materials Research Laboratory Central Facilities at the University of Illinois, where electron microscopy support was provided by Changqiang Chen and Honghui Zhou. The authors acknowledge the use of facilities and instrumentation supported by NSF through the University of Illinois Materials Research Science and Engineering Center DMR-1720633. Computational resources were funded by the National Science Foundation under Award Numbers DMR-1555278 and DMR-1720633. This research used resources of the Oak Ridge Leadership Computing Facility, which is a DOE Office of Science User Facility supported under Contract DE-AC05-00OR22725.

REFERENCES

(1) Setter, N.; Damjanovic, D.; Eng, L.; Fox, G.; Gevorgian, S.; Hong, S.; Kingon, A.; Kohlstedt, H.; Park, N. Y.; Stephenson, G. B.; Stolitchnov, I.; Taganstev, A. K.; Taylor, D. V.; Yamada, T.; Streiffer, S. Ferroelectric Thin Films: Review of Materials, Properties, and Applications. *J. Appl. Phys.* **2006**, *100*, 051606.

(2) Catalan, G.; Lubk, A.; Vlooswijk, A.; Snoeck, E.; Magen, C.; Janssens, A.; Rispens, G.; Rijnders, G.; Blank, D. H.; Noheda, B. Flexoelectric Rotation of Polarization in Ferroelectric Thin Films. *Nat. Mater.* **2011**, *10*, 963−967.

(3) Pompe, W.; Gong, X.; Suo, Z.; Speck, J. Elastic Energy Release due to Domain Formation in the Strained Epitaxy of Ferroelectric and Ferroelastic Films. *J. Appl. Phys.* **1993**, *74*, 6012−6019.

(4) Chen, C.; Liu, H.; Lai, Q.; Mao, X.; Fu, J.; Fu, Z.; Zeng, H. Large-Scale Domain Engineering in Two-Dimensional Ferroelectric $CuInP_2S_6$ *via* Giant Flexoelectric Effect. *Nano Lett.* **2022**, *22*, 3275−3282.

(5) Zhou, Y.; Guo, C.; Dong, G.; Liu, H.; Zhou, Z.; Niu, B.; Wu, D.; Li, T.; Huang, H.; Liu, M.; Min, T. Tip-Induced In-Plane Ferroelectric Superstructure in Zigzag-Wrinkled $BaTiO_3$ Thin Films. *Nano Lett.* **2022**, *22*, 2859−2866.

(6) Lu, H.; Bark, C.-W.; Esque de los Ojos, D.; Alcala, J.; Eom, C. B.; Catalan, G.; Gruverman, A. Mechanical Writing of Ferroelectric Polarization. *Science* **2012**, *336*, 59−61.

(7) Lipatov, A.; Chaudhary, P.; Guan, Z.; Lu, H.; Li, G.; Crégut, O.; Dorkenoo, K. D.; Proksch, R.; Cherifi-Hertel, S.; Shao, D.-F.; Tsymbal, E. Y.; Íñiguez, J.; Sinitskii, A.; Gruverman, A. Direct Observation of Ferroelectricity in Two-Dimensional MoS_2. *npj 2D Mater. Appl.* **2022**, *6*, 18.

(8) Heo, Y.; Sharma, P.; Liu, Y.; Li, J.; Seidel, J. Mechanical Probing of Ferroelectrics at the Nanoscale. *J. Mater. Chem. C* **2019**, *7*, 12441−12462.

(9) Wang, B.; Lu, H.; Bark, C. W.; Eom, C.-B.; Gruverman, A.; Chen, L.-Q. Mechanically Induced Ferroelectric Switching in $BaTiO_3$ Thin Films. *Acta Mater.* **2020**, *193*, 151−162.

(10) Wang, X.; Cui, A.; Chen, F.; Xu, L.; Hu, Z.; Jiang, K.; Shang, L.; Chu, J. Probing Effective Out-of-Plane Piezoelectricity in van der Waals Layered Materials Induced by Flexoelectricity. *Small* **2019**, *15*, 1903106.

(11) Haque, M. F.; Snapp, P.; Kim, J. M.; Wang, M. C.; Bae, H. J.; Cho, C.; Nam, S. Strongly Enhanced Electromechanical Coupling in Atomically Thin Transition Metal Dichalcogenides. *Mater. Today* **2021**, *47*, 69−74.

(12) Brennan, C. J.; Koul, K.; Lu, N.; Yu, E. T. Out-of-plane Electromechanical Coupling in Transition Metal Dichalcogenides. *Appl. Phys. Lett.* **2020**, *116*, 053101.

(13) Seo, J.; Kim, Y.; Park, W. Y.; Son, J. Y.; Jeong, C. K.; Kim, H.; Kim, W.-H. Out-of-Plane Piezoresponse of Monolayer MoS_2 on Plastic Substrates Enabled by Highly Uniform and Layer-Controllable CVD. *Appl. Surf. Sci.* **2019**, *487*, 1356−1361.

(14) Roy, R.; Nečas, D.; Zajíčková, L. Evidence of Flexoelectricity in Graphene Nanobubbles Created by Tip Induced Electric Field. *Carbon* **2021**, *179*, 677−682.

(15) Lee, C.; Wei, X.; Kysar, J. W.; Hone, J. Measurement of the Elastic Properties and Intrinsic Strength of Monolayer Graphene. *Science* **2008**, *321*, 385−388.

(16) Li, X.; Sun, M.; Shan, C.; Chen, Q.; Wei, X. Mechanical Properties of 2D Materials Studied by *In Situ* Microscopy Techniques. *Adv. Mater. Interfaces* **2018**, *5*, 1701246.

(17) Zhao, J.; Deng, Q.; Ly, T. H.; Han, G. H.; Sandeep, G.; Rümmeli, M. H. Two-Dimensional Membrane As Elastic Shell with Proof on the Folds Revealed by Three-Dimensional Atomic Mapping. *Nat. Commun.* **2015**, *6*, 8935.

(18) Guo, Y.; Qiu, J.; Guo, W. Mechanical and Electronic Coupling in Few-Layer Graphene and hBN Wrinkles: A First-Principles Study. *Nanotechnology* **2016**, *27*, 505702.

(19) Han, E.; Yu, J.; Annevelink, E.; Son, J.; Kang, D. A.; Watanabe, K.; Taniguchi, T.; Ertekin, E.; Huang, P. Y.; van der Zande, A. M. Ultrasoft Slip-Mediated Bending in Few-Layer Graphene. *Nat. Mater.* **2020**, *19*, 305−309.

(20) Yu, J.; Han, E.; Hossain, M. A.; Watanabe, K.; Taniguchi, T.; Ertekin, E.; van der Zande, A. M.; Huang, P. Y. Designing the Bending Stiffness of 2D Material Heterostructures. *Adv. Mater.* **2021**, *33*, 2007269.

(21) Xiao, J.; Zhu, H.; Wang, Y.; Feng, W.; Hu, Y.; Dasgupta, A.; Han, Y.; Wang, Y.; Muller, D. A.; Martin, L. W.; Hu, P.; Zhang, X.

Intrinsic Two-Dimensional Ferroelectricity with Dipole Locking. *Phys. Rev. Lett.* **2018**, *120*, 227601.
(22) Soleimani, M.; Pourfath, M. Ferroelectricity and Phase Transitions in α-In_2Se_3 van der Waals Material. *Nanoscale* **2020**, *12*, 22688−22697.
(23) Tao, X.; Gu, Y. Crystalline−Crystalline Phase Transformation in Two-Dimensional In_2Se_3 Thin Layers. *Nano Lett.* **2013**, *13*, 3501−3505.
(24) Huang, Y.-T.; Chen, N.-K.; Li, Z.-Z.; Wang, X.-P.; Sun, H.-B.; Zhang, S.; Li, X.-B. Two-Dimensional In_2Se_3: A Rising Advanced Material for Ferroelectric Data Storage. *InfoMat* **2022**, No. e12341.
(25) Zheng, X.; Han, W.; Yang, K.; Wong, L. W.; Tsang, C. S.; Lai, K. H.; Zheng, F.; Yang, T.; Lau, S. P.; Ly, T. H.; et al. Phase and Polarization Modulation in Two-Dimensional In_2Se_3 *via In Situ* Transmission Electron Microscopy. *Sci. Adv.* **2022**, *8*, No. eabo0773.
(26) Liu, Z.; Zheng, Q.-S.; Liu, J. Z. Stripe/Kink Microstructures Formed in Mechanical Peeling of Highly Orientated Pyrolytic Graphite. *Appl. Phys. Lett.* **2010**, *96*, 201909.
(27) Ren, M.; Liu, Z.; Zheng, Q.-s.; Liu, J. Z. Mechanical Buckling Induced Periodic Kinking/Stripe Microstructures in Mechanically Peeled Graphite Flakes from HOPG. *Acta Mech. Sin.* **2015**, *31*, 494−499.
(28) Rooney, A. P.; Li, Z.; Zhao, W.; Gholinia, A.; Kozikov, A.; Auton, G.; Ding, F.; Gorbachev, R. V.; Young, R. J.; Haigh, S. J. Anomalous Twin Boundaries in Two Dimensional Materials. *Nat. Commun.* **2018**, *9*, 3597.
(29) Plummer, G.; Rathod, H.; Srivastava, A.; Radovic, M.; Ouisse, T.; Yildizhan, M.; Persson, P. O. A.; Lambrinou, K.; Barsoum, M. W.; Tucker, G. J. On the Origin of Kinking in Layered Crystalline Solids. *Mater. Today* **2021**, *43*, 45−52.
(30) Zhou, Y.; Wu, D.; Zhu, Y.; Cho, Y.; He, Q.; Yang, X.; Herrera, K.; Chu, Z.; Han, Y.; Downer, M. C.; Peng, H.; Lai, K. Out-of-Plane Piezoelectricity and Ferroelectricity in Layered α-In_2Se_3. *Nano Lett.* **2017**, *17*, 5508−5513.
(31) Ding, W.; Zhu, J.; Wang, Z.; Gao, Y.; Xiao, D.; Gu, Y.; Zhang, Z.; Zhu, W. Prediction of Intrinsic Two-Dimensional Ferroelectrics in In_2Se_3 and Other III_2-VI_3 van der Waals Materials. *Nat. Commun.* **2017**, *8*, 14956.
(32) Cui, C.; Hu, W.-J.; Yan, X.; Addiego, C.; Gao, W.; Wang, Y.; Wang, Z.; Li, L.; Cheng, Y.; Li, P.; et al. Intercorrelated In-Plane and Out-of-Plane Ferroelectricity in Ultrathin Two-Dimensional Layered Semiconductor In_2Se_3. *Nano Lett.* **2018**, *18*, 1253−1258.
(33) Li, C.; Li, Y.; Tang, Y.; Zheng, S.; Zhang, J.; Zhang, Y.; Lin, L.; Yan, Z.; Jiang, X.; Liu, J.-M. Band structure, Ferroelectric Instability, and Spin−Orbital Coupling Effect of Bilayer α-In_2Se_3. *J. Appl. Phys.* **2020**, *128*, 234106.
(34) Gu, Y.; Hong, Z.; Britson, J.; Chen, L.-Q. Nanoscale Mechanical Switching of Ferroelectric Polarization *via* Flexoelectricity. *Appl. Phys. Lett.* **2015**, *106*, 022904.
(35) Das, S.; Wang, B.; Paudel, T. R.; Park, S. M.; Tsymbal, E. Y.; Chen, L.-Q.; Lee, D.; Noh, T. W. Enhanced Flexoelectricity at Reduced Dimensions Revealed by Mechanically Tunable Quantum Tunnelling. *Nat. Commun.* **2019**, *10*, 537.
(36) Ming, W.; Huang, B.; Zheng, S.; Bai, Y.; Wang, J.; Wang, J.; Li, J. Flexoelectric Engineering of van der Waals Ferroelectric $CuInP_2S_6$. *Sci. Adv.* **2022**, *8*, No. eabq1232.
(37) Kang, P.; Wang, M. C.; Knapp, P. M.; Nam, S. Crumpled Graphene Photodetector with Enhanced, Strain-Tunable, and Wavelength-Selective Photoresponsivity. *Adv. Mater.* **2016**, *28*, 4639−4645.
(38) Kumar, S.; Suryanarayana, P. Bending Moduli for Forty-Four Select Atomic Monolayers from First Principles. *Nanotechnology* **2020**, *31*, 43LT01.
(39) Timoshenko, S.; Woinowsky-Krieger, S. *Theory of Plates and Shells*; McGraw-Hill: New York, 1959; Vol. *2*.
(40) Lim, C.; Wang, C.; Kitipornchai, S. Timoshenko Curved Beam Bending Solutions in Terms of Euler-Bernoulli Solutions. *Arch. Appl. Mech* **1997**, *67*, 179−190.
(41) deWit, R. Theory of Disclinations: IV. Straight Disclinations. *J. Res. Natl. Bur. Stand., Sect. A* **1973**, *77*, 607.
(42) Metzger, C.; Rémi, S.; Liu, M.; Kusminskiy, S. V.; Castro Neto, A. H.; Swan, A. K.; Goldberg, B. B. Biaxial Strain in Graphene Adhered to Shallow Depressions. *Nano Lett.* **2010**, *10*, 6−10.
(43) Li, Y.-J.; Wang, J.-J.; Ye, J.-C.; Ke, X.-X.; Gou, G.-Y.; Wei, Y.; Xue, F.; Wang, J.; Wang, C.-S.; Peng, R.-C.; Deng, X.-L.; Yang, Y.; Ren, X.-B.; Chen, L.-Q.; Nan, C.-W.; Zhang, J.-X. Mechanical Switching of Nanoscale Multiferroic Phase Boundaries. *Adv. Funct. Mater.* **2015**, *25*, 3405−3413.
(44) Zhang, Y.; Kim, Y.; Gilbert, M. J.; Mason, N. Electronic Transport in a Two-Dimensional Superlattice Engineered *via* Self-Assembled Nanostructures. *npj 2D Mater. Appl.* **2018**, *2*, 31.
(45) Kresse, G.; Furthmüller, J. Efficiency of *Ab-Initio* Total Energy Calculations for Metals and Semiconductors Using a Plane-Wave Basis Set. *Comput. Mater. Sci.* **1996**, *6*, 15−50.
(46) Blöchl, P. E. Projector Augmented-Wave Method. *Phys. Rev. B* **1994**, *50*, 17953−17979.
(47) Monkhorst, H. J.; Pack, J. D. Special Points for Brillouin-Zone Integrations. *Phys. Rev. B* **1976**, *13*, 5188−5192.

https://doi.org/10.1021/acsnano.3c01311
ACS Nano XXXX, XXX, XXX−XXX